Geomechanics and Engineering, *Vol. 36, No. 3 (2024) 205-215*
https://doi.org/10.12989/gae.2024.36.3.205

Automatic detection of discontinuity trace maps: A study of image processing techniques in building stone mines

Mojtaba Taghizadeh*[1], Reza Khalou Kakaee[1], Hossein Mirzaee Nasirabad[2] and Farhan A. Alenizi[3]

[1]*Department of Mining, Petroleum and Geophysics Engineering, Shahrood University of Technology, Shahrood, Iran*
[2]*Department of Mining Engineering, Sahand University of Technology, Tabriz, Iran*
[3]*Department of Electrical Engineering, College of engineering, Prince Sattam Bin Abdulaziz University, Al-Kharj 11942, Saudi Arabia*

(*Received September 3, 2023, Revised November 20, 2023, Accepted November 21, 2023*)

Abstract. Manually mapping fractures in construction stone mines is challenging, time-consuming, and hazardous. In this method, there is no physical access to all points. In contrast, digital image processing offers a safe, cost-effective, and fast alternative, with the capability to map all joints. In this study, two methods of detecting the trace of discontinuities using image processing in construction stone mines are presented. To achieve this, we employ two modified Hough transform algorithms and the degree of neighborhood technique. Initially, we introduced a method for selecting the best edge detector and smoothing algorithms. Subsequently, the Canny detector and median smoother were identified as the most efficient tools. To trace discontinuities using the mentioned methods, common preprocessing steps were initially applied to the image. Following this, each of the two algorithms followed a distinct approach. The Hough transform algorithm was first applied to the image, and the traces were represented through line drawings. Subsequently, the Hough transform results were refined using fuzzy clustering and reduced clustering algorithms, along with a novel algorithm known as the farthest points' algorithm. Additionally, we developed another algorithm, the degree of neighborhood, tailored for detecting discontinuity traces in construction stones. After completing the common preprocessing steps, the thinning operation was performed on the target image, and the degree of neighborhood for lineament pixels was determined. Subsequently, short lines were removed, and the discontinuities were determined based on the degree of neighborhood. In the final step, we connected lines that were previously separated using the method to be described. The comparison of results demonstrates that image processing is a suitable tool for identifying rock mass discontinuity traces. Finally, a comparison of two images from different construction stone mines presented at the end of this study reveals that in images with fewer traces of discontinuities and a softer texture, both algorithms effectively detect the discontinuity traces.

Keywords: building stone mines; degree of neighborhood; hough transform; image processing; rock mass discontinuities

1. Introduction

A rock mass comprises intact rock and discontinuities, including joints, bedding-parallel discontinuities, faults, and other planes of weakness (Ren *et al*. 2022, Yao *et al*. 2023, Ren *et al*. 2023, Chen *et al*. 2023, Wu *et al*. 2022). To analyze the effect of fractures on the hydraulic and mechanical behavior of the rock mass, it is essential to characterize the fracture geometry at the exposed rock faces (Priest 1993, Dong *et al*. 2023). Understanding and analyzing the impact of discontinuities on rock engineering behavior is one of the most crucial tasks in mining engineering, as it greatly influences the stability of rock slopes and underground mineral or constructional spaces (Xu *et al*. 2022, Li *et al*. 2022a, Li *et al*. 2023, Ma *et al*. 2023, Liu *et al*. 2023). The impact of discontinuities on the engineering characteristics of the rock mass is more significant than the role intact rock can play in this context (Wu *et al.* 2011, Berisavljevic *et al.* 2023). In numerous engineering applications, these discontinuities are regarded as critical factors that influence the behavior of the rock mass, affecting aspects like the resistance of rock structures and the quality of fluid flow within it. In various other applications, including underground water transfer through aquifers, nuclear waste disposal tank construction, and oil and gas movement in hydrocarbon reservoirs, the network of rock mass fractures plays a pivotal role (Li *et al*. 2022b, Yang *et al*. 2022, Zhou *et al*. 2022, Li *et al*. 2022c, Yu *et al*. 2021). As a result, obtaining information about the structure of the rock mass is essential for optimizing the design and addressing rock engineering challenges.

Today, machine learning methods have shown a high ability to solve complex engineering problems (Cheng *et al*. 2023, Tao *et al*. 2023, Shi *et al*. 2023, Tie *et al*. 2023).

Image processing is a science-based machine learning technology that has primarily developed within the fields of electrical and computer engineering, but it has also found applications in geo-engineering sciences in recent years (Liu *et al*. 2021, Dong *et al*. 2023b, Zhou *et al*. 2022a, b, c). Geologists commonly employ aerial and satellite images to identify rock units, geological structures, and other features within the study area (Priest 1993). Image processing enables the evaluation of the RQD and the geological strength index (GSI) of underground rock mass (Saricam

*Corresponding author, M.Sc.
E-mail: mojtabataghizadeh2080@gmail.com

ISSN: 2005-307X (Print), 2092-6219 (Online)

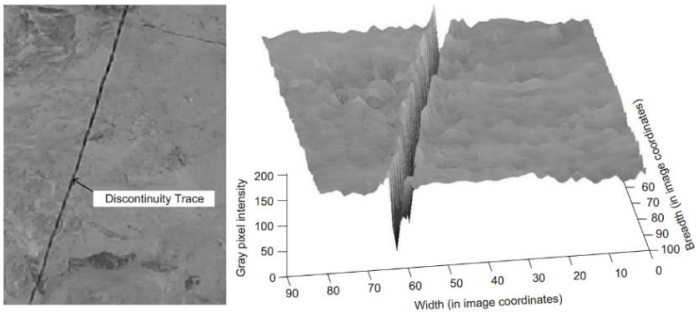

Fig. 1 Digital gray-scale and image intensity contour plot (Deb *et al.* 2008).

and Ozturk 2018). The applications of image processing in telemetry are substantial and continually expanding. One of its widely adopted applications involves large-scale regional surveys using satellite images for mining exploration (Noori and Panda 2016). As for the rock explosion analysis, the process of crack initiation, crack expansion as well as the crushing of rock fragments caused by the explosion of explosives could be momentarily scrutinized through using digital imaging .By using image processing and 3D laser scanner, it is possible to obtain special shapes and surfaces of explosive parts and use them for improving the accuracy of the fragmentation size distribution and calculation of fragmentation energy in blasting (Li *et al.* 2021, Zhang *et al.* 2023). Regarding the slope stability of open pit mines, it is possible to identify the areas that show displacement behavior by using image processing and investigate the potential of various types of failure on them (Kemeny *et al.* 2006). In the coal mine road excavation discussion, it is possible to identify the trace line of cross joints using image processing and obtain the Q and RMR system scores and utilize them to analyze the roof stability (Yuan *et al.* 2022).

Using the image processing and three-dimensional data structuring the Length distribution trace in the simple flat & uneven rock surface models as well as the mean discontinuity spacing distribution can be determined (Lee *et al.* 2022, Moomivand and Allahverdizadeh 2021, Cardo *et al.* 2022). Also, with the aid from 3D-image processing and Triaxial compression test, the rock fracture areas can be predicted (Chen *et al.* 2022). In underground mines, the displacement of the upper layers of the mine can be obtained using image processing (Ghabraie *et al*. 2015).

High-speed imaging techniques can be used to characterize the generated micro & macro-cracks under Brazilian loading (Khadivi 2023). Also, image processing can help determining the distribution of soil pores (Wang *et al.* 2016). In civil engineering, by using image processing and 3D reconstruction, the parameters of foam concrete pore structure can be calculated and used to analyze porous materials. And it is also possible to obtain the morphological characteristics of recycled brick-concrete (Liu and Liu 2021, Ma *et al.* 2021).

At the beginning of this study, a method for selecting the best edge detector and smoother was introduced. As a result, the Canny detector and median smoother were identified as the most effective. To detect the trace of discontinuity lines using the Hough transform, the image initially underwent a pre-processing operation, followed by an edge detection process on the resulting image. Following that, morphological operations were applied to the image to remove short edges. Subsequently, the Hough transform algorithm was applied to the image, revealing the trace lines through line drawing. Afterward, the results of the Hough transform were refined using both fuzzy clustering and reduced clustering algorithms. Upon completing this step, the process of identifying trace lines was finished, enabling the extraction of the desired geometric parameters from the image.

Another algorithm for detecting the trace of discontinuity lines have been determined based on the degree of neighborhood. In this algorithm, similar to the previous one, the target image undergoes pre-processing, followed by edge detection using the Canny detector and expansion of the detected edges. From this point onward, this algorithm adopts a different approach compared to the previous one. Initially, the thinning operation was applied to the study image, followed by the determination of the degree of neighborhood for lineament pixels. Subsequently, short lines were removed, and discontinuity lines were determined based on the degree of neighborhood. In the final step, the previously separated lines were reconnected using the method described below.

This study focuses on a rock mass of construction stone ore, identifying its discontinuity lines using image processing techniques and the application of two distinct algorithms. Ultimately, the discontinuity traces in two images related to constructional stone ore mines were identified using the aforementioned algorithms, and their efficiencies were compared. These algorithms were implemented in MATLAB software, automating all the joint detection stages.

2. Detection of traces of discontinuities line from the image

In a digital photo, traces of discontinuity lines can be identified due to sudden changes in the gray area values of the pixels. The human eye struggles to readily recognize and process these abrupt changes in pixel intensity. In Fig. 1, the trace of a discontinuity line in a fracture and the corresponding adjacent changes in pixel intensity are depicted. It is evident from this figure that changes in the

gray area values of pixels are easily distinguishable. However, such differentiation is not always feasible for all discontinuities. Often, due to the presence of noise or small crack openings, these joints are not easily identifiable to the naked eye, while image processing algorithms excel in detecting cracks, even with very subtle traces of discontinuity lines (Deb *et al*. 2008). In this article, the initial step involves conducting pre-processing on a sample image, employing both median and average filters. Subsequently, the image edges are detected using various detectors, and the best combination of smoother and detector is determined based on recognition and error rates.

3. Choosing the best edge detector and smoother

The purpose of pre-processing is to eliminate extraneous information before entering the processing stage. Specifically, it involves eliminating the influence of texture. Prior to the edge detection process, it is necessary to enhance the image in terms of both light intensity and noise. Noise, small joints, and microcracks need to be removed from the image.

When considering various edge detection and smoothing techniques, selecting the optimal method can be challenging. Typically, the selection of the best method depends on the obtained results and user judgment. A successful algorithm is more likely to correctly detect pixels representing the trace of discontinuity lines, while incorrect detections are possible, albeit with lower probability. This criterion can be defined using two parameters: recognition rate and error rate, as outlined by Hadjigerorgiou *et al*. (2003):

Recognition rate: The set of trace of discontinuity line pixels that are recognized as "correct" divided by the total number of trace discontinuity line pixels.

Error rate: The set of detected pixels that are not trace of discontinuities lines divided by the total number of pixels in the image.

In this article, in order to choose the best combination of edge detection and smoother, the above parameters were used. For this purpose, the recognition rate and the error rate of the combined algorithm with different mask sizes calculated for Fig. 2 is given in Table 1. For each edge detection algorithm, a certain a threshold has been specified to achieve the lowest error rate and the highest recognition rate. In this paper, the edges compared include Sobel, Prewitt, Roberts, Laplacian of a Gaussian (LOG), Zero crossings, and Canny. The smoothers applied comprise both median and average smoothers.

Although the numbers contained in Table 1 are for one image (Fig. 2) and are not true for other images, but the process is almost the same in the analysis of other images, so the following general points could be inferred:

- Canny's method, when paired with the median smoother, exhibits the lowest error percentage and the highest recognition rate.
- The LOG and Zero crossings methods demonstrate the lowest recognition rates and the highest error percentages.

Fig. 2 The image used to select the combination of the best edge detection and smoother algorithm

- As the mask size increases, the median smoother exhibits a lower error percentage compared to the average smoother.
- The median smoother achieves a higher recognition rate than the average smoother.
- As the mask size increases, the recognition rate decreases, and the error rate generally decreases as well (except for Roberts).

As indicated in Table (1), this paper utilized a 5×5 mask size with a median smoother and a Canny detector.

4. Provisioning the photo of the understudy rock mass

A digital camera was used to provide for the photo of the understudy facies in this article. The image undergoing various procedures in this study is an image of Par Tavousi marble construction stone mine located in Korei area of Arsanjan city, Fars province, Iran. Fig. 3(a) is the image on which the discussed study processes were performed.

4.1 Pre-processing operation

The purpose of pre-processing is to remove noise and reduce the texture effects. Considering section (3) in this article, a median filter with a mask size of 5x5 was used. Fig. 3(b) shows the effect of pre-processing operations.

4.2 Detecting the photo edges

In image processing, the algorithm detecting the edges in an image is called an edge detector. An edge detector takes a digital image as input and outputs an edge map, which in fact is a binary image (Dougherty 2009). After improving the image through the mentioned operations, those edges in the image representing the joints existing in the facies should be identified. As shown in section (3) of the article, a Canny detector with a high threshold of 0.2 and a low threshold of 0.08 was used. Fig. 3(c) illustrates the result of edge detection using Canny algorithm.

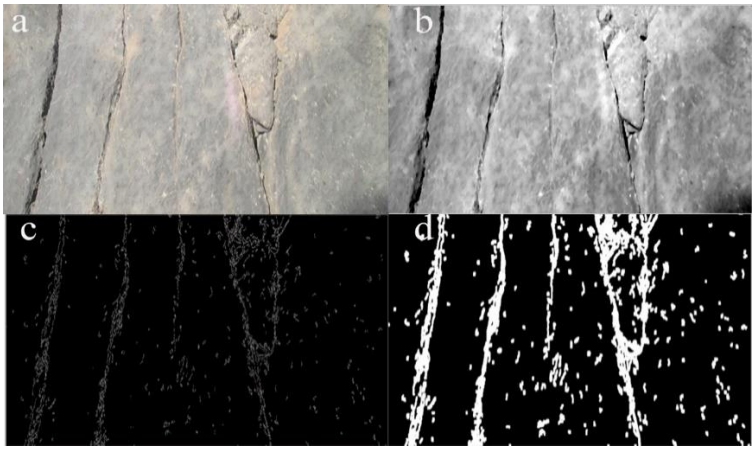

Fig. 3 (a) The main image of Marmatite construction stone mine, (b) Performing pre-processing operations with the median filter, (c) The output of the canny algorithm with a low threshold value of 0.08 and an upper threshold of 0.2 and (d) The image from the dilation operation

Table 1 Recognition Rate and error rate of Fig. 2 with edge detector, smoother and different mask sizes

edge detection algorithm			smoother	
Mask size	Recognition Rate (%)	Error rate (%)	Recognition Rate (%)	Error rate **(%)**
Sobel	Average Filter		Median Filter	
15×15	10/54	0/97	16/17	0/6
10×10	11/43	1/02	32/38	0/7
7×7	25/67	1	37/22	0/9
5×5	38/26	1/03	40/43	1/17
Prewitt	Average Filter		Median Filter	
15×15	10/3	0/95	16/1	0/59
10×10	11/32	1/01	32/27	0/68
7×7	25/29	1	37/4	0/88
5×5	38/3	1/03	40/65	1/14
canny	Average Filter		Median Filter	
15×15	10/24	1/4	13/18	13/18
10×10	15/13	1/7	23/14	23/14
7×7	42/67	1/68	65/11	65/11
5×5	73/89	1/8	87/1	87/1
Roberts	Average Filter		Median Filter	
15×15	11/54	0/97	16/62	1/8
10×10	13/61	0/93	30/14	0/76
7×7	28/5	0/9	60/73	0/79
5×5	54/06	0/78	65/93	1/04
Zero crossings	Average Filter		Median Filter	
15×15	10/1	2/13	15/61	1/75
10×10	12/53	2/24	25/62	2/16
7×7	21/54	3/03	31/21	3/06
5×5	29/58	4/8	34/13	4/81
Laplacian Of a Gaussian (LOG)	Average Filter		Median Filter	
15×15	10/1	2/13	15/61	1/75
10×10	12/53	2/25	25/62	2/16
7×7	21/54	3/02	31/21	3/06
5×5	29/58	4/8	34/13	4/81

4.3 Morphology operation

Next, the image obtained via Canny's algorithm was subjected to morphological operations. This operation includes three dilation, labeling connected components and thinning (Gonzalez and Woods 2004). The dilation operation makes the binary image thicker. This will connect the edges that are separated but belong to the same joint. Fig. 3(d) shows the effect of dilation operation.

5. Line detection through Hough transform algorithm

One of the methods of finding and connecting pixels in the form of lines is through Hough transform method. Hough transform is often used to detect lines in images resulting from edge detection, and using it, there is good possibility to detect other geometric shapes (e.g., circles and ellipses, etc.).

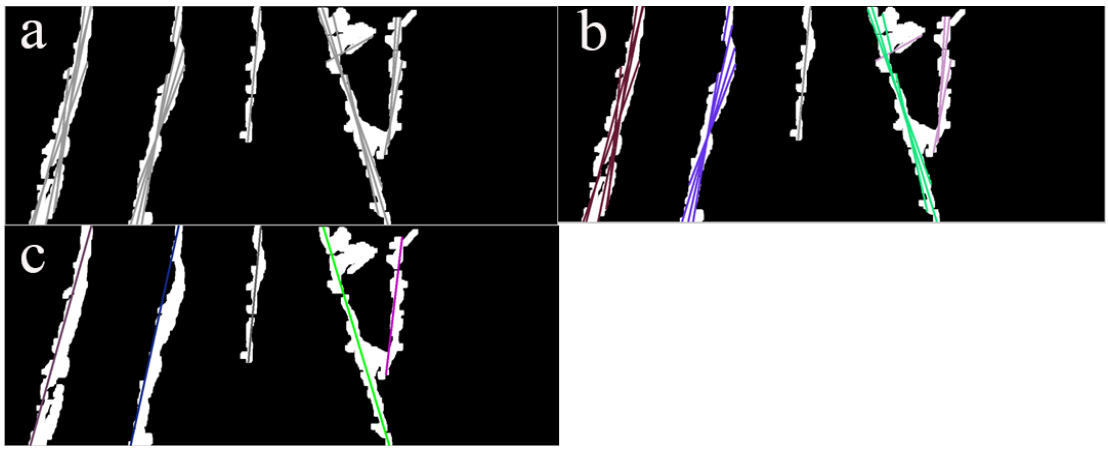

Fig. 4 (a) The results of Hough transform algorithm administration, (b) The results of Fuzzy C-Mean (FCM) and subtractive clustering (c) The results of farthest points algorithm

A line segment can be described in the image space with two quantities of slope and width from the origin

$$y_i = mx_i + c \quad (1)$$

where m is the slop and c is the width from origin. In Hough transform, the point (x_i, y_i) and all the lines that cross it are desirable. Indefinit lines cross the point (x_i, y_i) each of which lies on the line of Eq. (1). This line can be displayed as a point in the parametric space (Hough space) without losing all the information, so each line in the image space is equal to a single point in the parameter space. Eq. (1) can be written as the following equation in parameter space (Gonzalez and Woods 2004, Burger and Burge 2009).

$$c = y_i - mx_i \quad (2)$$

In this equation, c and m are constant and y_i and x_i are variable, and this relationship is the equation of a line in parameter space.

5.1 Line detection using Hough transform

After detecting the edges, a suitable algorithm should be used to detect the lines. We used Hough transform algorithm for this purpose. In the Hough transform, a straight line can be defined by the normal angle to the line (θ) and its distance from the origin (ρ). Also, this method can display separated edges as a line. The input of this algorithm is the minimum line length and the minimum distance between isolated edges. These parameters are considered to be 20 and 5 cm in this study respectively, and can be changed in accordance with the user's choice. Fig. 4(a) is the result of administering this algorithm. This algorithm outputs the coordinates of the beginning and end of the lines, the normal angle of each line and the distance from the origin. We used them as described below. In fact, the normal angle on the line is the angle of the trace of discontinuity line, and the values of this angle are independent of the orientation of the rock mass and the camera angle (Deb *et al*. 2008).

The problem of the Hough transform algorithm according to the Fig. 4(a) is that the number of detected lines for each joint is large, while each joint should be represented by one line. In the following, the improvement of the lines identified by the Fuzzy C-Mean (FCM) is discussed.

In order to show all lines of a joint with one line, all of them should be clustered with one number. To use the Fuzzy C-Mean (FCM), it is necessary to know the number of clusters and the input data. To select the appropriate input data, several parameters were given as input to the algorithm and by comparing the results, the input data were selected for the following two parameters (the data must be normalized before entering the function):

a) Slope of the lines (θ resulting from the Hough transform);

b) The width from the origin which is calculated for all the lines.

To implement this process, the following steps must be followed:

A) Calculation of the number of clusters with an initial step of 0.06 for the convergence radius.

B) Increasing the radius of convergence by 0.01 and recalculating the number of clusters.

C) Increasing the radius of convergence by 0.01 of the previous value and recalculating the number of clusters.

D) Comparison of the number of obtained clusters: If the number of clusters is equal, it is considered as the final number of clusters.

Next, the number of clusters is obtained and the input data matrix (slope and width from the origin of the lines) is given to the fuzzy clustering algorithm. The output of this algorithm constitutes the center and cluster membership function matrix. The highest value of membership function of each line is considered as its cluster. Fig. 4(c) shows the results of subtractive clustering and fuzzy clustering. In this figure, the identical clusters are in same color.

As can be seen in Fig. 4(c), it is obvious that the input parameters were suitable for joint detection and the algorithm was able to distinguish the lines belonging to a joint well. Now each joint should be represented with a line. To achieve this purpose, the following steps are taken:

A) Getting the coordinates of all the lines of a cluster.

B) Calculation of the distance between the beginning and the end of all lines relative to each other.

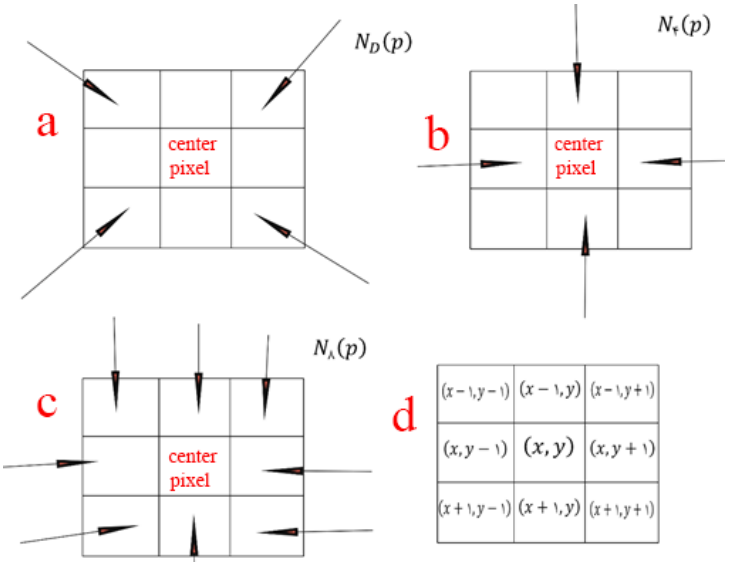

Fig. 5 Neighborhood types (a) 4-neighbors, (b) diagonal neighbors and (c) 8-neighbors coordinates

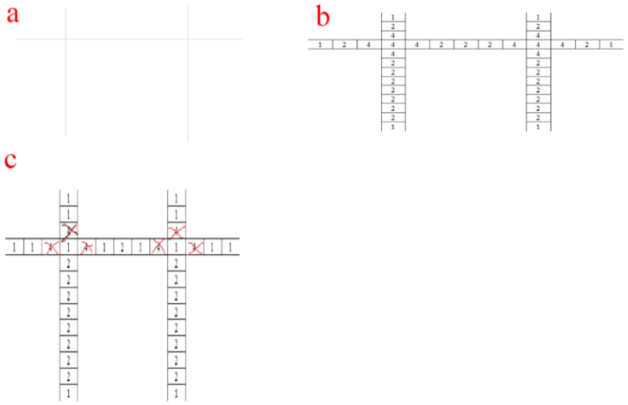

Fig. 6 The process of determining the neighborhood degree of pixels: (a) The trace of discontinuities line, (b) The degree of neighborhood of traces and (c) The degree of neighborhood of traces after removal of the neighborhood degree 3 and above and updating it

c) Calculation of the points that have the greatest distance to each other.

D) Connecting these points on the condition that they have the same label or the labels having the shortest distance to each other.

This algorithm is called the farthest points' algorithm, the results of which are shown in Fig. 4(d).

Fig. 4(d) shows that the extra lines have been removed and only one line has remained as the representative of each joint. Indeed, this algorithm, places the curved parts as well in the line so that there is no need to straighten the curved lines. Here, the traces lines detection process using the Hough transform is over. In the following, the algorithm for determining the degree of neighborhood is discussed.

6. Determining the lineaments degree of neighborhood

A pixel with (x,y) coordinates has four horizontal and vertical neighbors. This set of pixels is called 4-neighbors and is displayed as N_4 (p). Each pixel is one-unit distance away from (x,y), and if (x,y) lies on the image border, some neighbors fall outside the digital image. Four diagonal neighbors are also indicated by N_D (p). These points together with 4-neighbors collectively are called the 8-neighbors and are shown by N_8 (p) (Gonzalez and Woods 2008). These neighborhoods are represented in Fig. 5.

In this study, a set of 8-neighborhood was considered and based on the pixels (discontinuities) around the central pixel a number is obtained, representing the degree of neighborhood. Since the image underwent thinning and has a width of 1 pixel, the maximum pixel neighborhood was 4, and this pixel, as well as pixels with a neighborhood degree of 3, corresponded to the points of intersection or branching of discontinuities. The neighborhood 2 corresponds to the discontinuity length pixels and the neighborhood 1 represents the end points of the discontinuity.

To determine the octet degree of neighborhood of the pixel, a mask (3×3) is considered whose center is on the point (x,y) and is defined according to Fig. 5(c). The number of pixels that are equa to one (except for the central

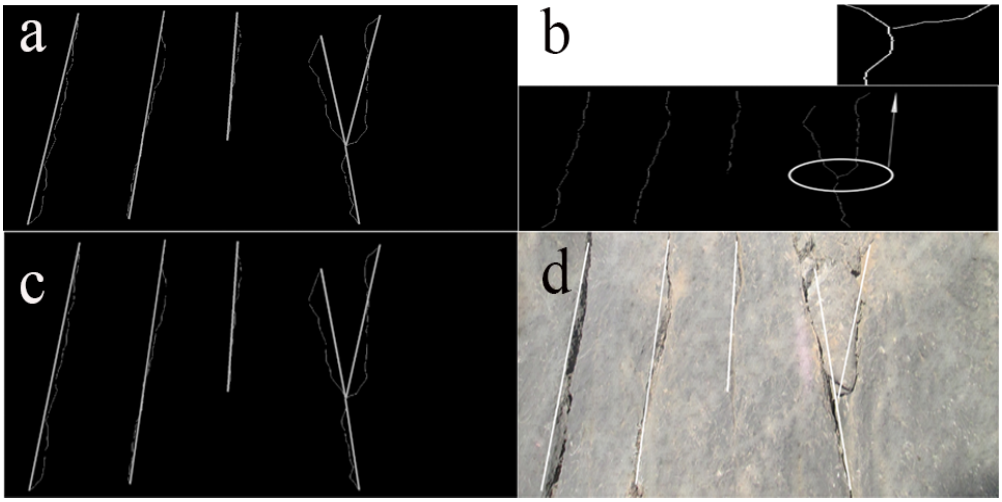

Fig. 7 (a) Result of the labeling the connected components and Removal short lines, (b) Connecting the separated lines, (c) Display of the discontinuity lines and (d) The results of algorithm on the original image

pixel) is considered as the neighborhood number of the pixel (x,y) and is stored in a matrix. In the boundaries where the neighborhood is outside the digital image, the points outside the image are considered as equal to zero. Since in pursuit of lines, the pixels with a neighborhood degree of 3 or higher cause problems, these pixels are removed and the pixel neighborhood degree information matrix is updated. It should be kept in mind that if a pixel is deleted, such deletion is taken into account when calculating the neighborhood degree of the next pixel. Finally, the coordinates of pixels with neighborhood degree of 1 are stored in a matrix.

This process is shown schematically in Fig. 6 and the relevant effect on the image contained in Fig. 4(b) is shown in Fig. 7(a).

6.1 Removal of short lines

After removing the neighborhood degree 3 and higher, some short length lines have been created which should be removed. At this stage, the labeling of the connected components was carried out once more and the lines with the length less than 5 cm were removed.

6.2 Display of the discontinuity lines

In this step, the discontinuity lines are detected and displayed with a line. Due to the removal of pixels with neighborhood degree of 3 and higher, there remain only the pixels with neighborhood degrees of 1 and 2. Pixels with a neighborhood degree of 1 are the endpoints of the trace lines, and pixels with a neighborhood degree of 2 lie along the trace lines. In section (9), the coordinates of the end pixels were stored in a matrix. In this step, the connected components are labeled first, and considering that there are two end pixels in each label, these points can be connected via drawing a line. This process is implemented by establishing a condition in the program that connects pixels with the same label and neighborhood degree of 1. The results of this process and section (9) are shown in Fig. 7(a).

6.3 Connecting the separated lines

Because of the described removal of the pixels with a neighborhood degree of 3 and higher in the image, the points that belong to a joint are separated from each other, which somehow should be re-connected to each other. This interruption causes many problems when determining the characteristics of discontinuities.

According to the obtained coordinates of the beginning and end of the lines, first the slope of all lines was calculated and stored, then the slope of all lines was compared with each other and the angle between them was obtained. Then the (shortest) distance between the lines was calculated and stored in the matrix. Now, according to the following process, the lines were connected to each other.

For the purpose of connecting the lines to each other, two conditions of the angle and the distance between the lines were considered. Hence, the lines having a distance of less than 2 cm (30 pixels) with the in-between angle of less than 10 degrees were recognized as eligible to be connected to each other. Now, if more than two lines are eligible, the two ones having the smallest angle in between them are considered. Fig. 7(b) illustrates the results of connecting the qualified lines.

The desired image still needs to be processed and the line of trace lines belonging to a single joint should be displayed with a single line. For this purpose, the neighborhood degree of pixels was calculated once again and the pixels with neighborhood degree of 3 and higher were removed. Afterwards, the labeling operation of the connected components was performed and the conditions of connecting the lines were examined. In the last stage of detection of lines, the end coordinates of the lineaments that are eligible for connection were stored in a matrix, and the farthest points of this matrix were calculated and considered as the coordinates of the beginning and end of a trace line and were connected to each other by drawing a line. The procedure results are shown in the Fig. 7(c). The results of running the described algorithm on the original image are shown in Fig. 7(d).

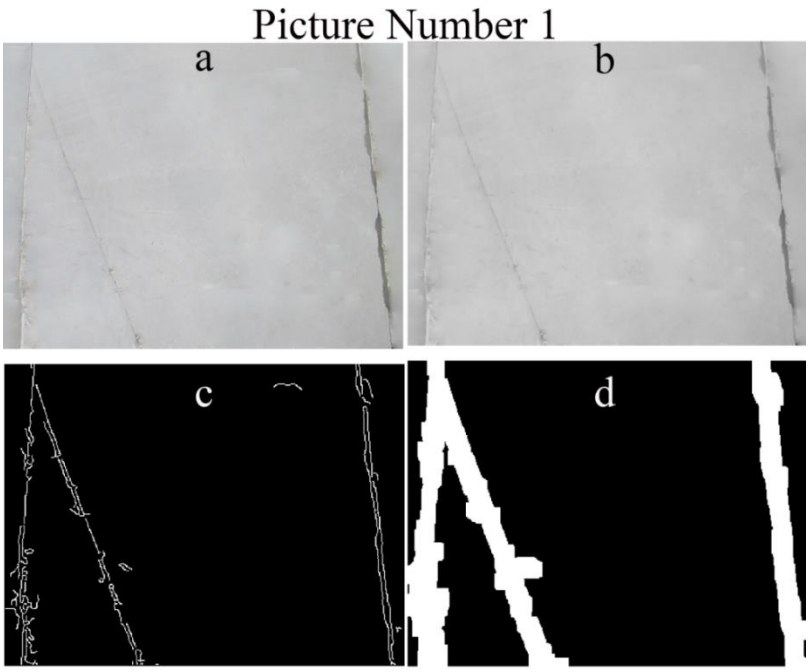

Fig. 8 Common steps of two algorithms (a) The main image, (b) Performing pre-processing operations with the median filter, (c) The output of the canny and (d) The image from of labeling the connected components and dilation operation

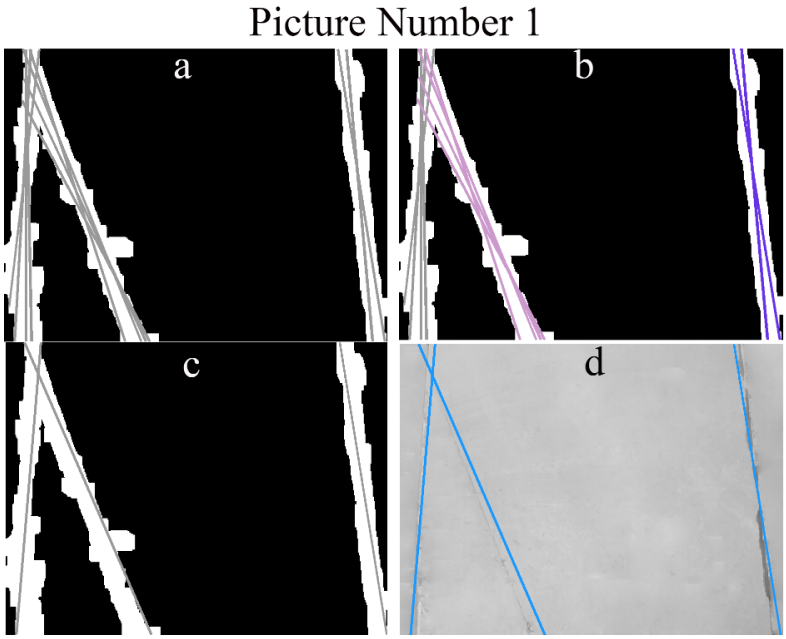

Fig. 9 The results of Hough transform algorithm (a) The results of Hough transform algorithm administration, (b) The results of Fuzzy C-Mean (FCM) and subtractive clustering, (c) The results of farthest points algorithm and (d) The results of Hough transform algorithm on the original image

7. Conclusions

This study introduces an automated method for detecting discontinuity traces in rock masses using image processing techniques. Initially, we compared various smoothers, edge detectors, and mask sizes by defining recognition rate and error rate parameters. As a result, we identified the median smoother, Canny detector, and a 5x5 mask size as the most effective options. In the initial shared steps of both algorithms, we conducted pre-processing operations to remove image noise through various spatial filters and subsequently identified edges using different detectors. From this point onward, each algorithm followed its distinct path. We employed the Hough transform algorithm to identify the discontinuity traces in the target image. Subsequently, we enhanced the Hough transform results using fuzzy clustering and reduced clustering methods. In the neighborhood degree method, we initially

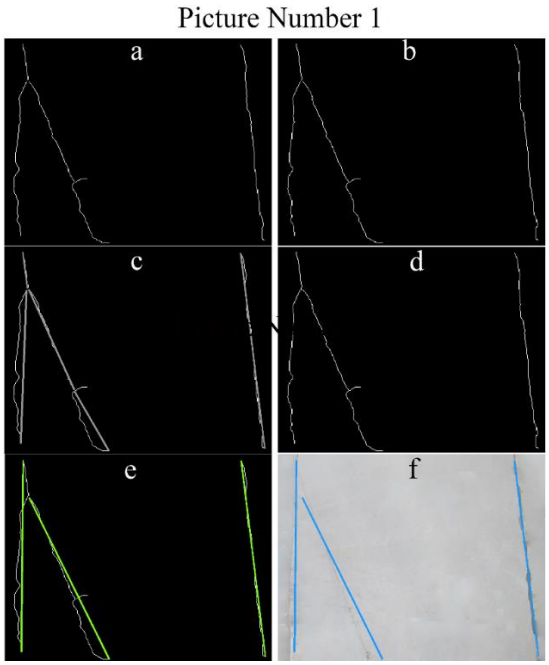

Fig. 10 results of degree of neighborhood (a) results of thinning operation (b) results of the degree of neighborhood of traces after removal of the neighborhood degree 3 and (c) result of the labeling the connected components and Removal short lines (d) Connecting the separated lines (e) Display of the discontinuity lines (f) The results of algorithm on the original image

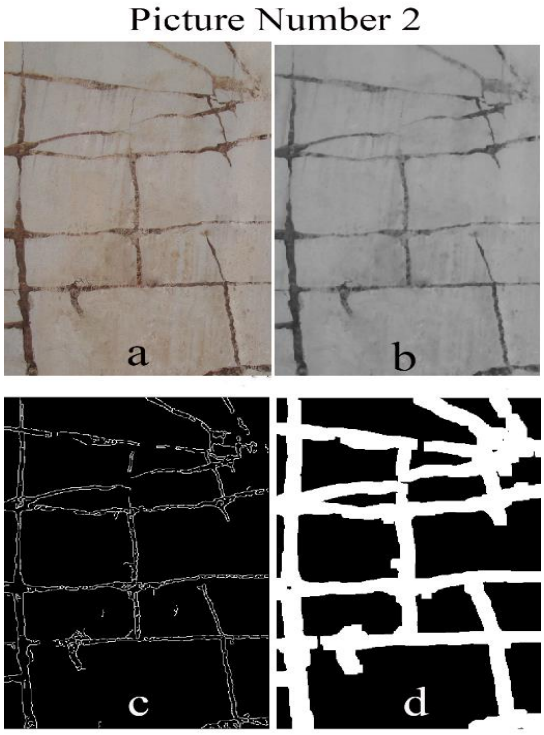

Fig. 11 Common steps of two algorithms (a) The main image (b) Performing pre-processing operations with the median filter (c) The output of the canny (d) The image from of labeling the connected components and dilation operation

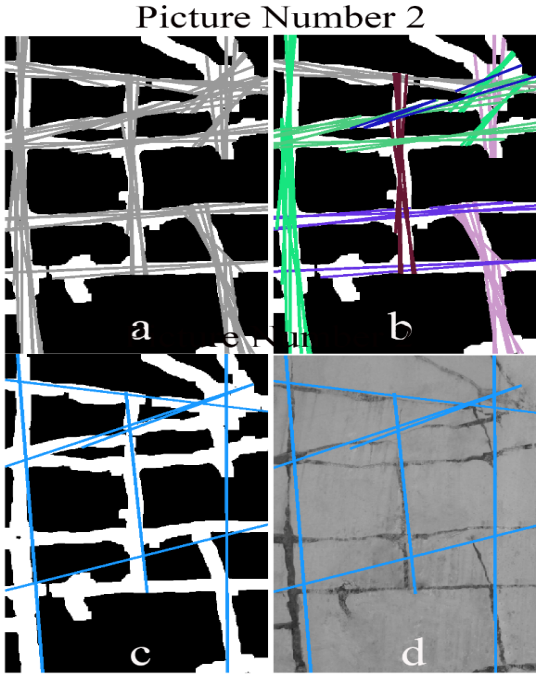

Fig. 12 The results of Hough transform algorithm **(**a) The results of Hough transform algorithm administration (b) The results of Fuzzy C-Mean (FCM) and subtractive clustering (c) The results of farthest points algorithm (d) The results of Hough transform algorithm on the original image

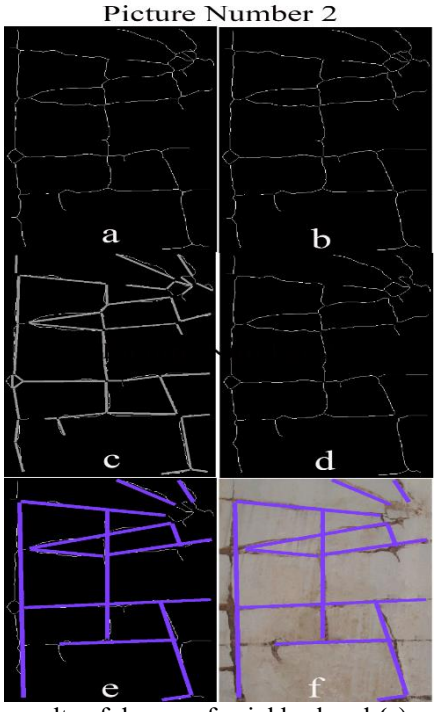

Fig. 13 results of degree of neighborhood **(**a) results of thinning operation (b) results of the degree of neighborhood of traces after removal of the neighborhood degree 3 and (c) result of the labeling the connected components and Removal short lines (d) Connecting the separated lines (e) Display of the discontinuity lines (f) The results of algorithm on the original image

performed a thinning operation on the target image and determined the degree of neighborhood for lineament pixels. We then removed short lines by re-labeling connected components and specified discontinuity traces based on the neighborhood degree. In the final stage, we connected the separated lines by establishing two conditions regarding the angle between the lines and the distance between them. This algorithm has been coded in MATLAB software so that all the joints detection procedures are performed automatically. Upon comparing the detected traces with the existing ones, we found that image processing is a valuable tool for identifying rock mass discontinuity traces. In the final part of this paper, two images of building stone mines are presented and the trace of discontinuities has been identified using the two mentioned algorithms. As a result of comparing the images, we can conclude that in images with a low number of traces and soft textures, both algorithms are proficient at trace detection. However, as image complexity and trace count increase, the neighborhood degree algorithm yields superior results.

Acknowledgments

This study is supported via funding from Prince Sattam bin Abdulaziz University project number (PSAU/2024/R/1445).

References

Berisavljevic, Z., Berisavljevic, D., Marjanovic, M. and Melentijevic, S. (2023), "Probabilistic analysis of anisotropic rock slope with reinforcement measures", *Geomech. Eng.*, **34**(3), 285–301. https://doi.org/10.12989/gae.2023.34.3.285.

Burger, W. and Burge, M.J. (2009), *Principles of Digital Image Processing*, **111**, London: Springer. https://doi.org/10.1007/978-1-84882-919-0.

Cardu, M., Godio, A., Oggeri, C. and Seccatore, J. (2022), "The influence of rock mass fracturing on splitting and contour blasts", *Geomech. Geoeng.*, **17**(3), 822-833. https://doi.org/10.1080/17486025.2021.1890234.

Chen, Y., Xu, J., Peng, S., Zhang, Q. and Chen, C. (2022), "Strain localization and seepage characteristics of rock under triaxial compression by 3D digital image correlation", *Int. J. Rock Mech. Min. Sci.*, **152**, 105064. https://doi.org/10.1016/j.ijrmms.2022.105064.

Chen, J., Wen, L., Bi, C., Liu, Z., Liu, X., Yin, L. and Zheng, W. (2023), "Multifractal analysis of temporal and spatial characteristics of earthquakes in Eurasian seismic belt", *Open Geosci.*, **15**(1). https://doi.org/10.1515/geo-2022-0482.

Cheng, Y., Lan, S., Fan, X., Tjahjadi, T., Jin, S. and Cao, L. (2023), "A dual-branch weakly supervised learning based network for accurate mapping of woody vegetation from remote sensing images", *Int. J. Appl. Earth Observ. Geoinform.*, **124**, 103499. https://doi.org/10.1016/j.jag.2023.103499.

Dong, W., Zhao, J., Qu, J., Xiao, S., Li, N., Hou, S. and Li, Y. (2023a), "Abundance matrix correlation analysis network based on hierarchical multihead self-cross-hybrid attention for hyperspectral change detection", *IEEE Trans. Geosci. Remote Sens.*, **61**, 1-13. https://doi.org/10.1109/TGRS.2023.3235401.

Dong, W., Yang, Y., Qu, J., Xiao, S. and Li, Y. (2023b), "Local information-enhanced graph-transformer for hyperspectral image change detection with limited training samples", *IEEE T. Geosci. Remote Sens.*, **61**, 1-14. https://doi.org/10.1109/TGRS.2023.3269892.

Deb, D., Hariharan, S., Rao, U.M. and Ryu, C.H. (2008), "Automatic detection and analysis of discontinuity geometry of rock mass from digital images", *Comput. Geosci.*, **34**(2), 115-126. https://doi.org/10.1016/j.cageo.2007.03.007.

Dougherty, G. (2009), *Digital Image Processing for Medical Applications*. Cambridge University Press.

Ghabraie, B., Ren, G., Smith, J. and Holden, L. (2015), "Application of 3D laser scanner, optical transducers and digital image processing techniques in physical modelling of mining-related strata movement", *Int. J. Rock Mech. Min. Sci.*, **80**, 219-230. https://doi.org/10.1016/j.ijrmms.2015.09.025.

Gonzales, R.C., Woods, R.E. and Eddins, S.L. (2004), *Digital Image Processing using MATLAB*. Pearson Prentice Hall.

Gonzalez, R.C. and Woods, R.E. (2002), *Digital Image Processing*. upper saddle River. J.: Prentice Hall.

Hadjigeorgiou, J., Lemy, F., Cote, P. and Maldague, X. (2003), "An evaluation of image analysis algorithms for constructing discontinuity trace maps". https://repository.geologyscience.ru/bitstream/handle/123456789/35239/Hadj_03.pdf?sequence=1.

Kemeny, J., Norton, B. and Turner, K. (2006), "Rock slope stability analysis utilizing ground-based LiDAR and digital image processing", *Felsbau*, **24**(3), 8-15. https://www.researchgate.net/publication/286549851_Rock_slope_stability_analysis_utilizing_groundbased_LIDAR_and_digital_image_processing.

Khadivi, B., Heidarpour, A., Zhang, Q. and Masoumi, H. (2023), "Characterizing the cracking process of various rock types under Brazilian loading based on coupled Acoustic Emission and high-speed imaging techniques", *Int. J. Rock Mech Min. Sci.*, **168**, 105417. https://doi.org/10.1016/j.ijrmms.2023.105417.

Lee, Y.K., Kim, J., Choi, C.S. and Song, J.J. (2022), "Semi-automatic calculation of joint trace length from digital images based on deep learning and data structuring techniques", *Int. J. Rock Mech. Min. Sci.*, **149**, 104981. https://doi.org/10.1016/j.ijrmms.2021.104981.

Li, R., Lu, W., Chen, M., Wang, G., Xia, W. and Yan, P. (2021), "Quantitative analysis of shapes and specific surface area of blasted fragments using image analysis and three-dimensional laser scanning", *Int. J. Rock Mech. Min. Sci.*, **141**, 104710. https://doi.org/10.1016/j.ijrmms.2021.104710.

Liu, C. and Liu, G. (2021), "Characterization of pore structure parameters of foam concrete by 3D reconstruction and image analysis", *Constr. Build. Mater.*, **267**, 120958. https://doi.org/10.1016/j.conbuildmat.2020.120958.

Li, R., Zhang, H., Chen, Z., Yu, N., Kong, W., Li, T., Wang, E., Wu, X. and Liu, Y. (2022a), "Denoising method of ground-penetrating radar signal based on independent component analysis with multifractal spectrum", *Measurement*, **192**, 110886. https://doi.org/10.1016/j.measurement.2022.110886.

Li, J., Wang, Y., Nguyen, X., Zhuang, X., Li, J., Querol, X., Li, B., Moreno, N., Hoang, V., Cordoba, P. and Do, V. (2022b), "First insights into mineralogy, geochemistry, and isotopic signatures of the Upper Triassic high-sulfur coals from the Thai Nguyen Coal field, NE Vietnam", *Int. J. Coal Geol.*, **261**, 104097. https://doi.org/10.1016/j.coal.2022.104097.

Li, Q., Lu, L., Zhao, Q. and Hu, S. (2022c), "Impact of inorganic solutes' release in groundwater during oil shale in situ exploitation", *Water*, **15**(1), 172. https://doi.org/10.3390/w15010172.

Li, J., Lin, Y., Nguyen, X., Zhuang, X., Li, B., Querol, X., Moreno, N. and Cordoba, P. (2023), "Enrichment of strategic metals in

the Upper Triassic coal from the Nui Hong open-pit mine, Thai Nguyen Coalfield, NE Vietnam", *Ore Geology Reviews*, **153**, 105301. https://doi.org/10.1016/j.oregeorev.2023.105301.

Liu, Q., Yuan, H., Hamzaoui, R., Su, H., Hou, J. and Yang, H. (2021), "Reduced reference perceptual quality model with application to rate control for video-based point cloud compression", *IEEE T. Image Process.*, **30**, 6623-6636. https://doi.org/10.1109/TIP.2021.3096060.

Liu, W., Zhou, H., Zhang, S. and Zhao, C. (2023), "Variable parameter creep model based on the separation of viscoelastic and viscoplastic deformations", *Rock Mech. Rock Eng.*, **56**(6), 4629-4645. https://doi.org/10.1007/s00603-023-03266-7.

Ma, S., Qiu, H., Yang, D., Wang, J., Zhu, Y., Tang, B., Sun, K. and Cao, M. (2023), "Surface multi-hazard effect of underground coal mining", *Landslides*, **20**(1), 39-52. https://doi.org/10.1007/s10346-022-01961-0.

Ma, K., Huang, X., Shen, J., Hu, M., Long, G., Xie, Y. and Zhang, W. (2021), "The morphological characteristics of brick-concrete recycled coarse aggregate based on the digital image processing technique", *J. Build. Eng.*, **44**, 103292. https://doi.org/10.1016/j.jobe.2021.103292.

Moomivand, H., Seadati, S. and Allahverdizadeh, H. (2021), "A new approach to improve the assessment of rock mass discontinuity spacing using image analysis technique", *Int. J. Rock Mech. Min. Sci.*, **143**, 104760. https://doi.org/10.1016/j.ijrmms.2021.104760.

Noori, O. and Panda, S.S. (2016). "Site-specific management of common olive: Remote sensing, geospatial, and advanced image processing applications", *Comput. Electron. Agr.*, **127**, 680-689. https://doi.org/10.1016/j.compag.2016.07.031.

Priest, S.D. (1993), *Discontinuity Analysis for Rock Engineering*. Springer Science & Business Media. https://doi.org/10.1007/978-94-011-1498-1.

Ren, C., Yu, J., Liu, S., Yao, W., Zhu, Y. and Liu, X. (2022), "A plastic strain-induced damage model of porous rock suitable for different stress paths", *Rock Mech. Rock Eng.*, **55**(4), 1887-1906. https://doi.org/10.1007/s00603-022-02775-1.

Ren, C., Yu, J., Zhang, C., Liu, X., Zhu, Y. and Yao, W. (2023), "Micro–macro approach of anisotropic damage: A semi-analytical constitutive model of porous cracked rock", *Eng. Fract. Mech.*, **290**, 109483. https://doi.org/10.1016/j.engfracmech.2023.109483.

Shi, Y., Xi, J., Hu, D., Cai, Z. and Xu, K. (2023), "RayMVSNet++: learning ray-based 1D implicit fields for accurate multi-view stereo", *IEEE T. Pattern Anal. Machine Intell.*, 1-17. https://doi.org/10.1109/TPAMI.2023.3296163.

Saricam, T. and Ozturk, H. (2018), "Estimation of RQD by digital image analysis using a shadow-based method", *Int. J. Rock Mech. Min. Sci.*, **112**, 253-265. https://doi.org/10.1016/j.ijrmms.2018.10.032.

Tao, Y., Shi, J., Guo, W. and Zheng, J. (2023), "Convolutional neural network based defect recognition model for phased array ultrasonic testing images of electrofusion joints", *J. Pressure Vessel T. - ASME*, **145**(2). https://doi.org/10.1115/1.4056836.

Tie, Y., Rui, X., Shi-Hui, S., Zhao-Kai, H. and Jin-Yu, F. (2023), "A real-time intelligent lithology identification method based on a dynamic felling strategy weighted random forest algorithm", *Petroleum Sci*., https://doi.org/10.1016/j.petsci.2023.09.011

Tian, W.L., Yang, S.Q., Dong, J.P., Cheng, J.L. and Lu, J.W. (2022), "An experimental study on triaxial failure mechanical behavior of jointed specimens with different JRC", *Geomech. Eng.*, **28**(2), 181-195. https://doi.org/10.12989/gae.2022.28.2.181.

Vaziri, M.R., Tavakoli, H. and Bahaaddini, M. (2022), "2D numerical study of the mechanical behaviour of non-persistent jointed rock masses under uniaxial and biaxial compression tests", *Geomech. Eng.*, **28**(2), 117-133. https://doi.org/10.12989/gae.2022.28.2.117

Wu, M., Ba, Z and Liang, J. (2022), "A procedure for 3D simulation of seismic wave propagation considering source-path-site effects: Theory, verification and application", *Earthq. Eng. Struct. D.*, **51**(12), 2925–2955. https://doi.org/10.1002/eqe.3708.

Wang, J., Guo, L., Bai, Z. and Yang, L. (2016). "Using computed tomography (CT) images and multi-fractal theory to quantify the pore distribution of reconstructed soils during ecological restoration in opencast coal-mine", *Ecol. Eng.*, **92**, 148-157. https://doi.org/10.1016/j.ecoleng.2016.03.029.

Wu, Q., Kulatilake, P.H.S.W. and Tang, H.M. (2011), "Comparison of rock discontinuity mean trace length and density estimation methods using discontinuity data from an outcrop in Wenchuan area, China", *Comput. Geotech.*, **38**(2), 258-268. https://doi.org/10.1016/j.compgeo.2010.12.003.

Xu, L., Cai, M., Dong, S., Yin, S., Xiao, T., Dai, Z., Wang, Y. and Reza Soltanian, M. (2022), "An upscaling approach to predict mine water inflow from roof sandstone aquifers", *J. Hydrology*, **612**, 128314. https://doi.org/10.1016/j.jhydrol.2022.128314.

Yuan, Y., Zhang, N., Han, C., Yang, S., Xie, Z. and Wang, J. (2022), "Digital image processing-based automatic detection algorithm of cross joint trace and its application in mining roadway excavation practice", *Int. J. Min. Sci. Tech.*, **32**(6), 1219-1231. https://doi.org/10.1016/j.ijmst.2022.09.009.

Yang, M., Wang, H., Hu, K., Yin, G. and Wei, Z. (2022), "IA-Net$:$ an inception–attention-module-based network for classifying underwater images from others", *IEEE J. Oceanic Eng.*, **47**(3), 704-717. https://doi.org/10.1109/JOE.2021.3126090.

Yao, W., Yu, J., Liu, X., Zhang, Z., Feng, X. and Cai, Y. (2023), "Experimental and theoretical investigation of coupled damage of rock under combined disturbance", *Int. J. Rock Mech. Min. Sci.*, **164**, 105355. https://doi.org/10.1016/j.ijrmms.2023.105355.

Yu, J., Zhu, Y., Yao, W., Liu, X., Ren, C., Cai, Y. and Tang, X. (2021). "Stress relaxation behaviour of marble under cyclic weak disturbance and confining pressures", *Measurement*, **182**, 109777. https://doi.org/10.1016/j.measurement.2021.109777.

Zhuo, Z., Du, L., Lu, X., Chen, J. and Cao, Z. (2022a), "Smoothed Lv distribution based three-dimensional imaging for spinning space debris", *IEEE T. Geosci. Remote Sens.*, **60**, 1-13. https://doi.org/10.1109/TGRS.2022.3174677.

Zhou, G., Li, H., Song, R., Wang, Q., Xu, J. and Song, B. (2022b), "Orthorectification of fisheye image under equidistant projection model", *Remote Sens.*, **14**(17), 4175. https://doi.org/10.3390/rs14174175.

Zhou, G., Liu, W., Zhu, Q., Lu, Y. and Liu, Y. (2022c). "ECA-MobileNetV3(Large)+SegNet model for binary sugarcane classification of remotely sensed images", *IEEE T. Geosci. Remote Sens.*, **60**, 1-15. https://doi.org/10.1109/TGRS.2022.3215802.

Zhou, G., Wang, Q., Huang, Y., Tian, J., Li, H. and Wang, Y. (2022d), "True2 Orthoimage Map Generation", *Remote Sens.*, **14**(17), 4396. https://doi.org/10.3390/rs14174396

Zhang, B., Li, Y., Yang, X.Y., Li, S.C., Wei, C. and Songa, J. (2023), "Influence of size and location of a pre-existing fracture on hydraulic fracture propagation path", *Geomech. Eng.*, **32**(3), 321. https://doi.org/10.12989/gae.2023.32.3.321.

IC